A Novel Approach to Design the Dual Rotor Switched Reluctance Motor Based Electric Vehicles

Majid Aryanezhad[1], Elahe Ostadaghaee[2]

[1]Shahid Chamran university of Ahvaz, Ahvaz, Iran
m.aryanezhad@gmail.com
[2]National Iranian Gas Company (NIGC), Jam, Iran
e.ostadaghaee@gmail.com

Abstract

Electric and hybrid electric vehicles are attractive candidates for sustainable transportation due to its higher efficiency and low emission. The critical choice on the electric motors is its capability of motoring and regenerative braking characteristics. Switched reluctance machines are viable candidate as with proper control and extended constant power range operation replacing the multi-gear transmission. Recently developed dual magnetic circuit reluctance machine configuration make it added advantage with its feasibility on the optimizing the magnetic flux flow. The dual magnetic circuit reluctance machines through double rotor is presented and compared with conventional machine for its power density. Further to evaluate the dynamic performance the proposed machine is compared with that of the conventional machine. It is found that the torque density of the proposed machine is 65% higher than that of the conventional machine and show promising candidate for the EV and HEV applications in the near future.

Keywords—SRM; dual rotor SRM; regenerative braking; electric vehicle

1. Introduction

A traction motor is usually controlled in such ways that the terminal voltage is linearly increased from zero speed to its base speed with the constant uniform magnetic field [1]. After the base speed the terminal voltage is kept constant and the magnetic field is weakened towards the critical speed before breaking down. The typical torque power speed characteristics required for traction motor is as shown in Fig.1. For EV applications the constant power range has to be extended for better efficiency and control [1,2]. Table 1 shows the electric vehicle models developed by various manufacturers.

Conventionally the magnet controlled machines are used due to its higher power density. DC motor drives are used traditionally due to their ability to achieve high torque at low speeds but drags rapid maintenance. Brushless DC machines (PMBLDC) in most modern on-road vehicles is primarily due to their maintenance free operation. Equally modern vehicles encompass Permanent Magnet Synchronous Machines (PMSM) as alternative due to their higher efficiency and power density over other type of electric motors [1,3]. The prime challenge of this machine is the flux weakening control at constant power high speed region. Induction motors is disadvantageous due to low efficiency due to the motor losses due the winding losses in the stator and rotor together with the challenge in recovering energy during braking.

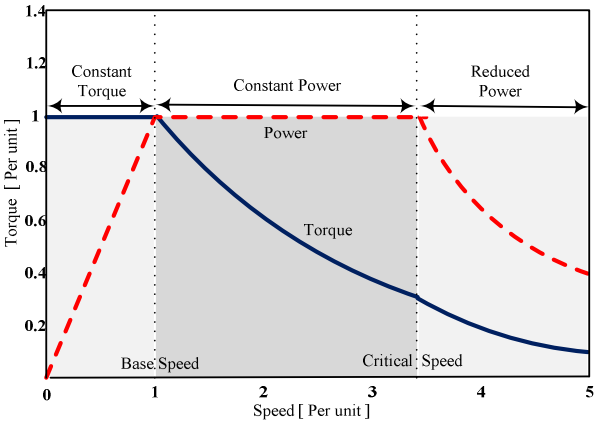

Fig.1 Torque Power Characteristics of the EV [1]

Table1 Electric vehicle models

Type of motor	Manufacture	Name
DC motor	Mazda	Bongo
	Fiat	Elettra
	Conceptor	G-Van
SRM	Lucas	Chloride
Induction motor	General Motors	EV1
	Ford	Think city
	Fiat	Seicento Elettra
PMSM	Toyota	RAV4
	Nissan	Altra
	Honda	EV Plus
PMDC motor	Suzuki	Senior tricycle
PMBLDC	Honda	Civis
	Toyota	Prius

Moving forward the usage on the high volume of the rare earth permanent magnet motors would push the motor manufacturers to the choice of the magnet less machines in the near future. Switched Reluctance machine (SRM) though simple in construction their design and control are challenging making it not the prime choice for commercial deployment [4,5,6]. Hence the key design challenges in the SR machine design are the better utilization of steel and copper, better electromagnetic flow through, the chosen machine topology and geometry to

achieve higher torque per unit weight for better performances. Recently the dual magnetic circuit design through double stator is proposed in [7,8]. Dual magnetic circuit can be done through introducing either a double stator configuration or through double rotor configurations [8]. In the double stator structure the electrical loading is doubled however it do not improve the efficiency as the resistance value increases and hence the copper loss. Also it increases the mass of the vehicle when the machine is on board, regenerative action invokes the reverse effect on the current flow in the two winding coil increasing the mutual inductance effect on the machine. This paper presents the dual circuit realization through a double rotor configuration. The design aspects, the magnetic circuit analysis using FEA tool and its performance analysis is presented.

2. Magnetic Flow Considerations

2.1. Design Aspects

The capability or ratings of the electric motors depends on the magnetic loading and the electric loading in the machine. The design process follows the design guidelines presented in [9]. The magnetic loading derives the peak fundamental component of the flux density in the motor air-gap and the electric loading derives the net ampere turns per unit periphery. The capability machine equation is as shown in Eq. (1) to Eq. (3).

Q=Magnetic loading (B_{avg})*Electric loading (ac) (1)

$$Q = 1.11\pi^2 k_c k_d (B_{avg} DL)(ac.D) n_s * 10^{-3} \quad (2)$$

$$Q = 1.11 k_c k_d (B_{avg} L)(ac) \frac{v_a^2}{n_s} * 10^{-3} \quad (3)$$

K_c, K_d, D, L, V_a and n_s are pitch factor, distribution factor, outer diameter of the machine, stack length, rotational speed and synchronous speed, respectively.

As mentioned earlier the increase in the electric loading is either through the optimizing the slot shape and conductor sizing. The magnetic loading depends on the optimizing the flux flow in the magnetic circuit. In SR machines the torque production depends on the rotor stator interactive positions. Hence most of the flux through the yoke to complete the magnetic circuit is utilized. The reluctance $\Re_g$ for the dual circuit for the Fig.2 is as shown in Eq. (4). As seen the reluctance is reduced through the magnetic circuit and the air gap length is reduced.

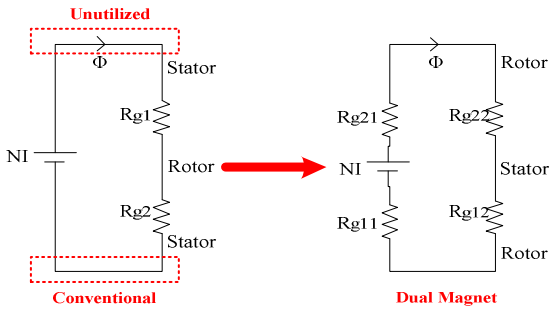

Fig.2 Evolution of dual air-gap circuit

$$\Re_g = \frac{\ell_{g1}}{2\mu_0 A_{g1}} + \frac{\ell_{g2}}{2\mu_0 A_{g2}} \quad (4)$$

2.2. Machine Structure

Fig.3(a) shows the proposed dual magnetic circuit realization through a double rotor structure. Both the inner and outer rotor is connected to the common shaft and rotates together. The stator is to encapsulate with a guide rails to hold the stampings together. The coils are wound around the stator poles and are connected for the long flux realization. Fig.3(b) shows the exploded view of the dual rotor reluctance machine proposed in this paper. Table 2 shows the parameters used in the design of the machine. For comparative analysis the conventional machine is also designed and analyzed for the same volume using the FEA tool.

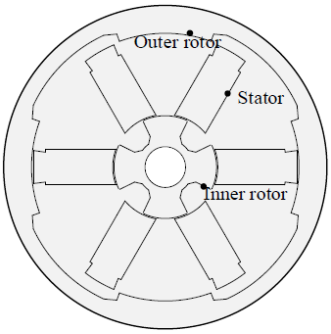

(a) Machine configurations

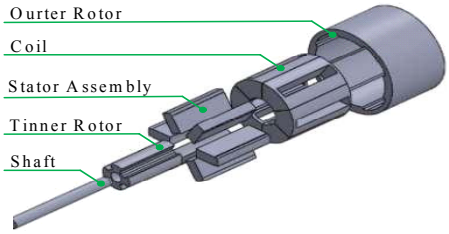

(b) Exploded view of the machine

Fig.3 Proposed dual rotor reluctance machine

Table2 Electric vehicle machine parameters

Parameter	Value
Outer Stator Diameter	65.8 mm
Inner Stator Diameter	25.8 mm
Inner Rotor Diameter	25.6 mm
Outer Rotor Diameter	80 mm
Stack Length	50 mm
Outer Rotor Inner Suface Diameter	66 mm
Shaft Diameter	10 mm
Inner air-gap Length	0.1 mm
Outer air-gap Length	0.1 mm
Outer Rotor Pole arc	40^0
Inner Rotor Pole arc	50^0
Stator Inner Pole arc	40^0
Stator Outer Pole arc	14.25^0

2.3. Finite element analysis by JMAG Simulator

To run the simulation the machine is constructed using the JMAG® simulation tools. After constructing the machine, the parameters values assigned to the machine is separated into model, study properties, materials, analysis conditions, circuit, and mesh generation. Fig.4 shows the steps used in simulation using the tool.

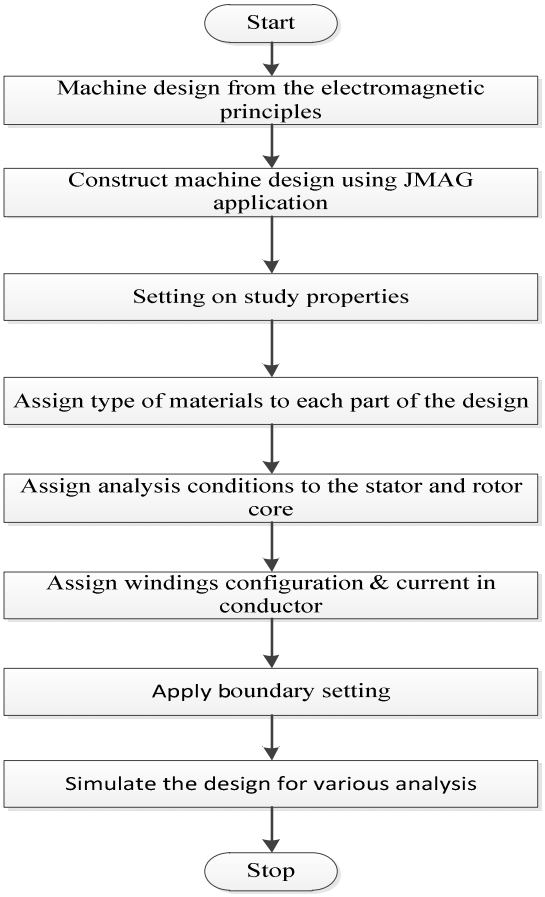

Fig.4 Procedure for FEA simulation

It is essential to derive the values of flux linkage and inductance at various rotor angles so that the sequence of excitation is effective to make the motor to continuously rotate. Since these machines operate close to saturation the switching frequency from the control design is critical. Hence, deriving the magnetic characteristics prior is important for advanced control such as feed-forward [10,11].

Fig.5 shows the typical inductance characteristics for motoring and braking (generation) and its range depends on the inductance profile, the configuration and pole geometry of the machine. It shows the inductance profile at various current excitations for rotor position. Fig.6 shows the magnetic flux flow at various position of the machine. The analysis is done for one rotor pole pitch and it is found the flux flow is uniform and the leakage is minimal. For electric vehicle operation it is highly important the recovery of energy during the braking (regeneration). Hence improving torque density with low ripple to a lower value make SR machines a significant choice for battery operated electric vehicles [12].

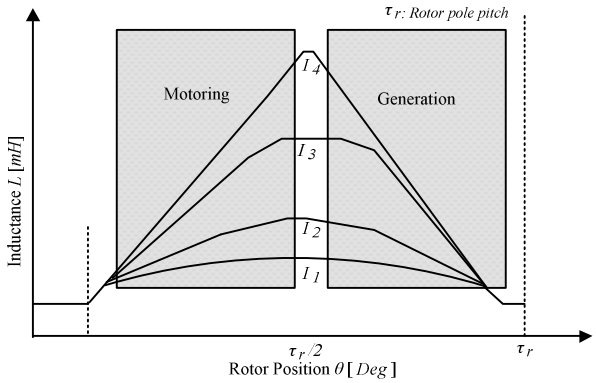

Fig.5 Motoring generating characteristics

3. Evaluation Parameters

In order to evaluate the performance of the proposed machine and also to comparatively study the performance with respect to the existing machines the following parameters are used.

3.1. Motor Constant Square Density (G)

The motor constant square density is one of the quality factors for comparison of machines as it involves the comparison based on the sizing of the machines. The motor constant square density is presented in Eq. (5)

$$\begin{cases} G = \dfrac{K_m^2}{V} \\ K_m = \dfrac{K_t}{\sqrt{P_{in}}} \\ K_t = \dfrac{T_{avg}}{I} \end{cases} \tag{5}$$

where K_m is the machine constant, K_t is the torque constant, V is the volume of the machine, T_{avg} is the average torque of the machine, P_{in} being the input electrical power.

3.2. Torque per Unit Volume (T_{mv})

The torque per unit volume is a rough constant value for motors, but it can vary widely over the full spectrum of motor that are available. The torque per unit volume T_{mv} is as shown in Eq. (6).

$$T_{mv} = \frac{4T_{avg}}{\pi D_{or}^2 L_{sk}} \tag{6}$$

where

D_{or} is the diameter of the outer rotor, L_{sk} is the stack length

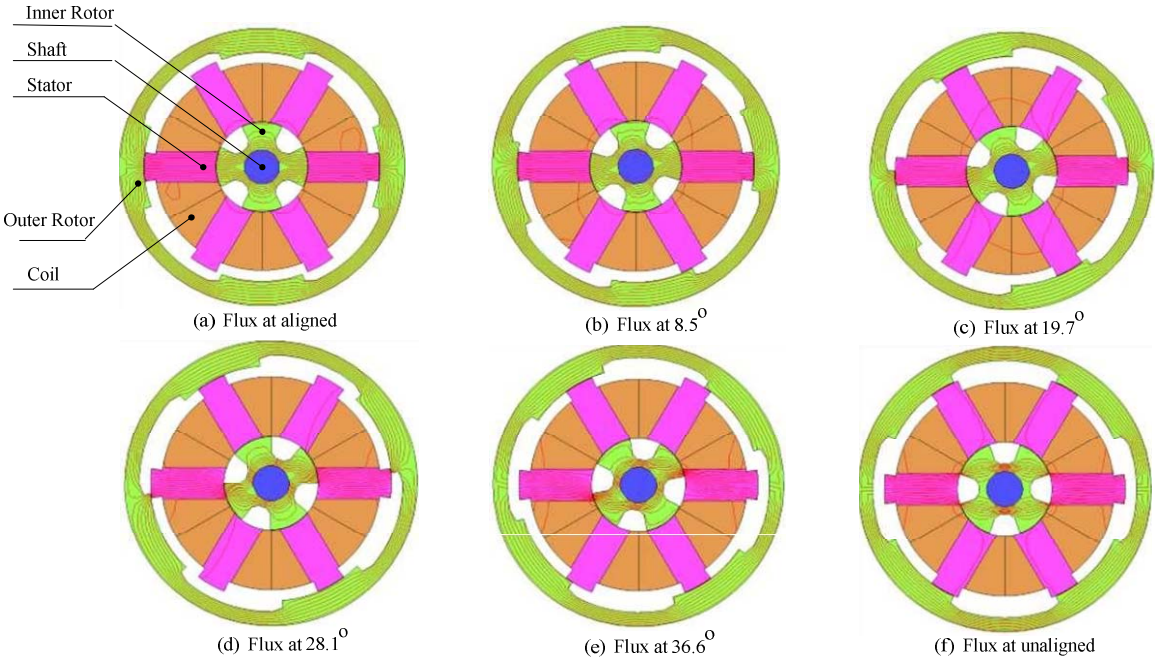

Fig.6 Magnetic flux flow inside the machine

3.3. Ripple Factor (γ_{rf})

The peak variations of the torque over a full cycle of operation of a motor is expressed as ripple factor as shown in Eq. (7).

$$\gamma_{rf} = \frac{T_{\max} - T_{\min}}{T_{avg}} \tag{7}$$

where T_{max} is the torque maximum of the machine and T_{min} is the torque minimum of the machine.

3.4. Total Harmonic Distortion (THD)

THD is used to assess the signal distortion by cause of oscillations at output harmonics characteristics is as shown in Eq. (8).

$$THD = \sqrt{\frac{\sum_{i=2}^{\infty} T_i^2}{T_1}} \tag{8}$$

where T_1 is the fundamental torque of the machine.

4. Results and Discussions

4.1. Static Characteristics

The flux linkage waveform of the proposed machine when excited with current of 3A, 5A, and 7A is as shown in Fig.7. The results shows that as the current is increasing the flux output are also increase proportionally. Close to the half pole pitch the magnetic flux is constant and hence need to use controller to switch on the next phase. This information is highly helpful in the design of the controller at later stage.

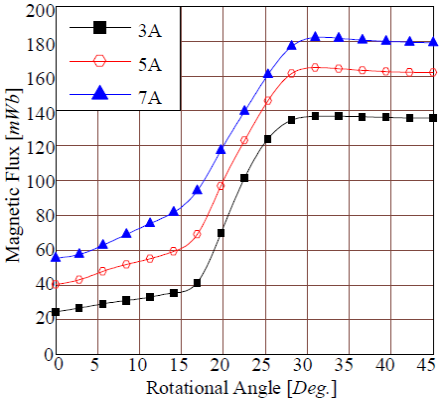

Fig.7 Magnetic flux characteristics

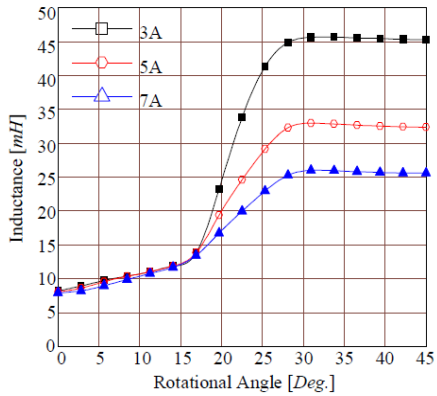

Fig.8 Inductance characteristics

Fig.8 shows the inductance characteristics for the proposed machines. In traction applications the large dead zone enables larger phase advance control so that enough phase current and hence enough torque is built up when the rotor speed is above the base speed. This is realized with smaller pole arc at unaligned position and small air gap at aligned position that is seen in out of design here.

4.2. Dynamic Characteristics

The excitation state is designed by shifting its condition between opening and closing switches in accordance with the position of the rotor. The timing operating of the alternating conditions influences the torque properties. During the excitation state, an increase torque average and torque constant is significant. Fig.9(a) shows the drive and the switching pattern used for the drive is shown in Fig.9(b).

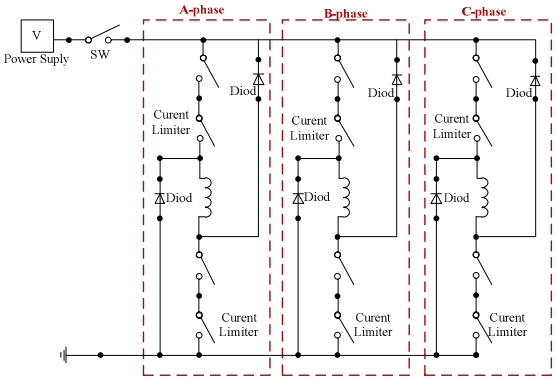

(a) Drive circuit diagram

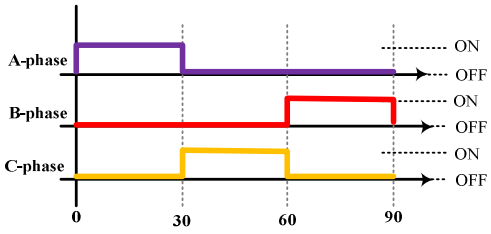

(b) Drive switched timing chart (rotation angle (deg.))

Fig.9 Drive switching used

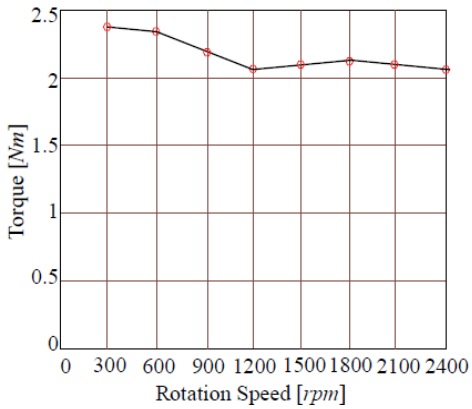

Fig.10 Speed torque characteristics

Fig.10 shows the speed torque characteristics of the proposed machines as the speed is varied from 0 to 2400 rpm.
For the four rotor pole with dual the speed settles close to 1500 rpm reaching torque close to 2.1 Nm. The maximum torque achieved is about 2.4 Nm. In Fig.11, efficiency is rises and peaks at 90% as the rotation speed is increased. The increase in the efficiency is because of the switching timing that was set with the accordance of rotation speed.

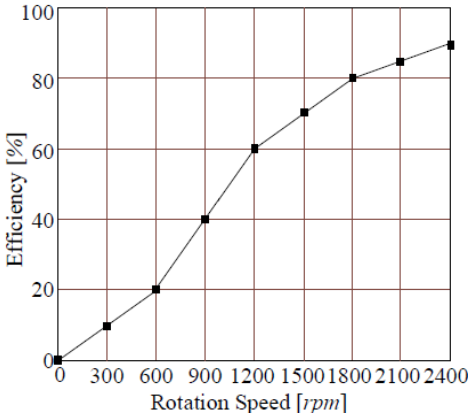

Fig.11 Efficiency versus speed

4.3. Comparative Evaluations

Table3 shows the comparative evaluations of the conventional SRM and the proposed dual rotor switched reluctance machine (DRSRM). Both machines are designed for same sizing and procedure. As seen from the results the comparison is made for the same volume, since no magnetic field from magnet is involved the electrical loading is decreased in DRSRM due to the space required for the second rotor. However the air gap is doubled, the net air gap length in both the machines are the same. The torque density is increased by 68% and the motor constant square density is increased by 65%. As mentioned earlier the motor constant square density is the best figure of merit to compare as it involves the volume and weight of the machines. The average torque in case of the DRSRM is increase by 36% as subsequently the analysis of the ripple is presented.

Table3 COMPARATIVE Evaluations

Figure of merit	**SRM**	**DRSRM**
Current , I (A)	5	5
Volume, V (m^3)	0.00213	0.00199
T_{avg} (N.m)	**1.26**	**1.98**
T_{max} (N.m)	**1.656**	**2.418**
T_{min} (N.m)	1.652	2.170
γ_{rf}	0.0032	0.13
T_{mv} (Nm/A)	**2366.2**	**3979**
K_t (Nm/A)	0.13	0.20
K_m (NM/A/(W)$^{-1/2}$)	0.013	0.020
G [(Nm)^2/A^2/W/m^3]	**0.07**	**0.20**

4.4. Torque Components in Regeneration Mode

Fig.12 shows the timing control used in the generating conditions.

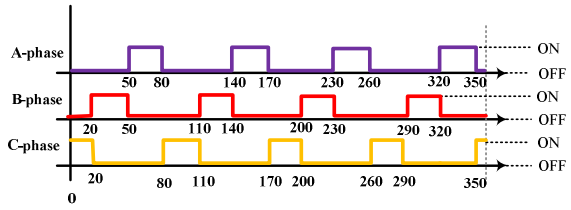

Fig.12 Ripple torque switch timing

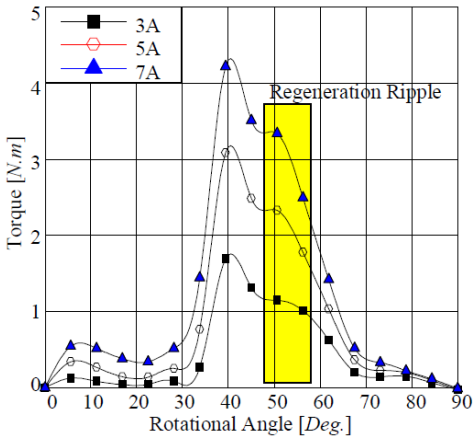

Fig.13 Ripple during regeneration

Fig.13 shows the toque characteristics used for analysis of the machine for consideration during regeneration. It is found the ripple is reduced when the angle of control is between 55^0-57^0 during regeneration and 10^0-12^0 during motoring. Here, a comparison results in terms of torque ripple and average torque for is presented in Table 4.

Table4 Torque and ripple during generation

θ_S(Deg)	Average T (%)		Ripple T (%)	
	SRM	DRSRM	SRM	DRSRM
55	73.95	**75.58**	94.48	**84.10**
56	69.01	**69.28**	91.13	**79.33**
57	64.07	**63.07**	87.36	**74.59**

5. Conclusions

Switched reluctance machines are viable candidate as with proper control and extended constant power range operation without multi-gear transmission. A dual magnetic circuit is realized through double rotor structure and the static and dynamic performance is presented. The proposed machine is compared with that of the conventional machines through motor constant square density, a factor used to compare for the same volume. It is found that the torque density of the proposed machine is 36% higher than that of the conventional machine with the motor constant density increased by 65 %. The ripple is reduced if the operation of the angle is done at 550-570 during regeneration and 100-120 during motoring. The proposed machine is showing as a promising candidate for the EV and HEV applications in the near future.

6. References

[1] Chu, C.L.; Tsai, M.C.; Chen, H.Y., "Torque control of brushless DC motors applied to electric vehicles," Electric Machines and Drives Conference, IEEE International, pp.82,87, 2001.

[2] Aryanezhad, M.; Ostadaghaee, E., Joorabian, M.; "Management and Coordination Charging of Smart Park and V2G Strategy Based on Monte Carlo Algorithm," Smart Grids Conference (SGC), pp.1-8, 9-10 Dec. 2014.

[3] Wang, T.; Cheng, M.; Fan, Y.; Chau, K.T, "A double stator permanent magnet brushless machine system for electric variable transmission in hybrid electric vehicles," in Proc. 2010 IEEE Vehicle Power Propulsion Conf., pp.1-5, Sep 1-3 2010.

[4] Hu, K.; Yi, P.; Liaw, C., "An EV SRM Drive Powered by Battery/Supercapacitor withG2V and V2H/V2G Capabilities," Industrial Electronics, IEEE Transactions on, vol..99, pp.1-11, 2015.

[5] Aida, S.; Komatsuzaki, A.; Miki, I., "Basic characteristics of electric vehicle using 40kW switched reluctance motor," Electrical Machines and Systems, International Conference on, pp.3358,3361, 17-20 Oct. 2008.

[6] Jazdzynski, W.; Majchrowicz, M., "An approach to find an optimum designed SRM for electric vehicle drive," Electrical Machines, 18th International Conference on, pp.1,6, 6-9 Sep. 2008.

[7] Abbasian, M.; Moallem, M.; Fahimi, B., "Double-Stator Switched Reluctance Machines (DSSRM): Fundamentals and Magnetic Force Analysis," Energy Conversion, IEEE Transactions on, vol.25, no.3, pp.589,597, Sep. 2010.

[8] Wei Peng.; Dong-Hee, Lee.; Fengge, Zhang.; Jin-Woo, Ahn., "Design and characteristic analysis of a novel bearingless SRM with double stator," Electrical Machines and Systems (ICEMS), 2011 International Conference on, pp.1,6, 20-23 Aug. 2011.

[9] Aravind Vaithilingam "Design of Electrical Apparatus" Charulatha Publications, Chennai, 2003.

[10] Hongwei, Gao.; Yimin, Gao.; Ehsani, M., "A neural network based SRM drive control strategy for regenerative braking in EV and HEV," Electric Machines and Drives Conference. IEEE International, pp.571,575, 2001.

[11] Yu, Guojun.; Cheng, He.; Huo, Yingjie., "Research on the switched reluctance machine drive system for electric vehicles," Electrical Machines and Systems (ICEMS), 2014 17th International Conference on, pp.192,197, 22-25 Oct. 2014.

[12] Aryanezhad, M.; Joorabian, M.; Ostadaghaee, E., "Modeling and Simulation of PHEV as a Virtual UPQC Based on Vehicle to Grid Technology", International Review on Modelling and Simulations (I.RE.MO.S.), Vol. 5, N. 4, pp.743,747, Aug. 2012.